RESEARCH ARTICLE

FASEB BioAdvances WILEY

In vivo optical assessment of cerebral and skeletal muscle microvascular response to phenylephrine

Laura Mawdsley[1,2] | Rasa Eskandari[1,3] | Farah Kamar[1,3] | Ajay Rajaram[4] | Lawrence C. M. Yip[1,3] | Naomi Abayomi[5] | Stephanie Milkovich[2] | Jeffrey J. L. Carson[1,3] | Keith St. Lawrence[1,3] | Christopher G. Ellis[1,2] | Mamadou Diop[1,3]

[1]Department of Medical Biophysics, Western University, London, Ontario, Canada

[2]Robarts Research Institute, Western University, London, Ontario, Canada

[3]Imaging Program, Lawson Health Research Institute, London, Ontario, Canada

[4]Boston Children's Hospital, Harvard Medical School, Boston, Massachusetts, USA

[5]School of Medicine, University of Ottawa, Ottawa, Ontario, Canada

Correspondence

Mamadou Diop, Department of Medical Biophysics, Western University, London, Ontario, Canada.
Email: mdiop@uwo.ca

Abstract

This study aimed to investigate the simultaneous response of the cerebral and skeletal muscle microvasculature to the same phenylephrine (PE) boluses. A hybrid optical system that combines hyperspectral near-infrared spectroscopy (hs-NIRS) and diffuse correlation spectroscopy (DCS) was used to monitor changes in tissue oxygenation and perfusion. Data were collected from the head and hind limb of seven male Sprague–Dawley rats while administering intravenous (IV) injections of PE or saline to all animals. The response to saline was used as a control. Skeletal muscle oxygenation decreased significantly after PE injection, while a statistically underpowered decrease in perfusion was observed, followed by an increase beyond baseline. Vascular conductance also decreased in the muscle reflecting the drug's vasoconstrictive effects. Tissue oxygenation and perfusion increased in the brain in response to PE. Initially, there was a sharp increase in cerebral perfusion but no changes in cerebral vascular conductance. Subsequently, cerebral flow and vascular conductance decreased significantly below baseline, likely reflecting autoregulatory mechanisms to manage the excess flow. Further, fitting an exponential function to the secondary decrease in cerebral perfusion and increase in muscular blood flow revealed a quicker kinetic response in the brain to adjust blood flow. In the skeletal muscle, PE caused a transient decrease in blood volume due to vasoconstriction, which resulted in an overall decrease in hemoglobin content and tissue oxygen saturation. Since PE does not directly affect cerebral vessels, this peripheral vasoconstriction shunted blood into the brain, resulting in an initial increase in oxygenated hemoglobin and oxygen saturation.

KEYWORDS

cerebral desaturation, diffuse correlation spectroscopy, near-infrared spectroscopy, phenylephrine, tissue oximetry

Laura Mawdsley and Rasa Eskandari are cofirst author.

1 | INTRODUCTION

Phenylephrine (PE) is a vasopressor commonly administered intravenously to increase mean arterial pressure (MAP) through vasoconstriction that elevates total peripheral resistance.[1,2] Despite the well-known effects of PE on MAP, its effects on the microcirculation are unclear, with reports of the drug either significantly decreasing microvascular oxygen saturation and blood flow,[3-6] or causing no change in different microvascular beds and patient populations.[7-9] Importantly, different organs, and even different regions within an organ,[10,11] are supplied by their own capillary bed with distinct structures and functions, metabolic demands, and autoregulatory mechanisms to control perfusion. Therefore, there is a need to determine the effects of PE on the skeletal muscle, where the drug causes vasoconstriction, as well as the brain microcirculation, where conflicting effects of the drug have been reported.

Importantly, resistance in large arteries and the microvasculature are both affected by circulating vasoconstrictors. In the skeletal muscle, PE binds to α-adrenergic receptors, thereby causing vasoconstriction.[12] This effect on the skeletal muscle is responsible for the increase in MAP observed with PE administrations. However, PE does not cross the blood–brain barrier[13] and cerebral vessels lack α-adrenergic receptors.[14] Despite the lack of evidence for having a direct impact on the brain, previous work using cerebral oximetry linked PE with cerebral desaturation.[14-16]

Most cerebral oximetry devices are based on continuous-wave near-infrared spectroscopy (NIRS), which has limited sensitivity to the adult brain due to signal contamination from the extracerebral layer (ECL; scalp and skull).[17,18] One explanation for the observed desaturation reported with PE administration is signal contamination from the strong vasoconstriction in the scalp,[19] thereby masking the true cerebral response to PE. This is supported by studies using NIRS technology with increased sensitivity to the brain that reported smaller magnitudes of cerebral desaturation.[14,16,20,21]

Rats are a good preclinical model for investigating cerebral events using NIRS because of their thin ECL. In NIRS, the concentrations of oxygenated and deoxygenated hemoglobin (HbO and Hb, respectively) are estimated noninvasively from measurements of light absorption by tissue. Tissue oxygen saturation (StO_2) can be quantified as the ratio of HbO to the total hemoglobin content (HbT = HbO + Hb). Furthermore, diffuse correlation spectroscopy (DCS) is another optical technique that can quantify changes in tissue perfusion as relative blood flow (rBF). By pairing these two optical modalities for concurrent measurements, the microcirculation can be assessed more comprehensively. We hypothesize that PE causes vasoconstriction in the muscle but not in the brain. The objective of this study was to use a hybrid hyperspectral (hs)-NIRS/DCS system to test this hypothesis by monitoring the responses the cerebral and muscle microvasculature to the same PE boluses.

2 | METHODS

2.1 | Animal protocol

This study was approved by the Animal Care and Use Committee at Western University. Data were collected from seven male Sprague Dawley rats (154.9 ± 7.7 g). The animals were anesthetized with sodium pentobarbital (65 mg/kg), and their carotid artery and jugular vein were cannulated for MAP measurements and intravenous (IV) fluid delivery, respectively. Subsequently, a tracheostomy was performed to aid the animals with breathing, and sufficient ventilation was confirmed through arterial blood sampling of pO_2, pCO_2 (maintained at ~40 mmHg), pH, and lactate with a VetScan i-STAT 1 (Abbott Laboratories, IL, USA). Core body temperature was maintained at 37 ± 0.5°C using a rectal temperature probe and a heat mat. Heart rate, temperature, and MAP were monitored continuously.

Each rat received up to six 0.1 mL IV injections of PE (10 mg/kg in 0.9% NaCl) and up to three 0.1 mL IV injections of saline (0.9% NaCl) for comparison as control. The PE dosage was determined based on previous work[20] that showed that this dose produces a similar response to the desired effect in humans. To ensure full dosing, the IV line was flushed with 0.1 mL of saline promptly after each injection.

2.2 | Optical instrument and data collection

A hybrid hs-NIRS/DCS system[22-26] was used to monitor the microvascular response to PE and saline boluses in both the skeletal muscle and brain of the rats. Identical probe holders (Figure 1A) were secured on the hind limb and scalp of each rat for simultaneous hs-NIRS and DCS monitoring with a source-detector separation (ρ) of 10 mm, to measure the global effects of the same PE bolus injection on the skeletal muscle and cerebral microvasculature, simultaneously. A bifurcated multimode fiber bundle (diameter = 2.5 mm, core = 400 μm, numerical aperture (NA) = 0.22; Thorlabs, NJ, USA) directed light from a 20-W broadband halogen lamp (HL-2000; Ocean Insight, FL, USA) to the scalp and hind limb. Two similar multimode fibers collected and directed diffusely reflected light from the two tissues to a Maya Pro spectrometer (Ocean Insight) and a QE 65000 spectrometer (Ocean Insight) for brain and muscle monitoring, respectively. A second bifurcated multimode fiber (diameter = 2.5 mm, core = 400 μm, numerical aperture
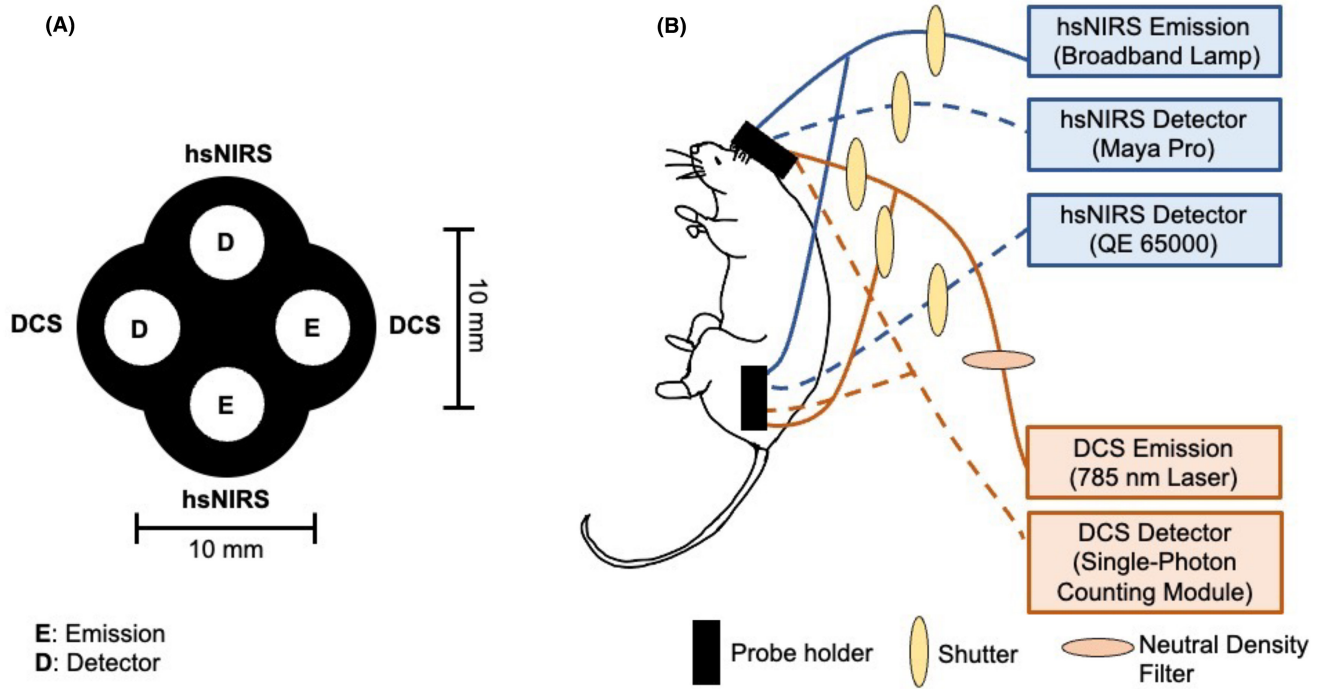
(A)

(B)

FIGURE 1 Simplified schematic of (A) probe holder and (B) hybrid hs-NIRS/DCS system. Solid lines in (B) represent emission while dashed lines are for detection. Schematic is not drawn to scale.

(NA) = 0.22; Thorlabs) bundle directed light from a 785 nm, long coherence length laser (CrystaLaser, NV, USA). A bifurcated optical probe with two single mode fibers (outer diameter = 2.5 mm, core = 4.4 μm, numerical aperture (NA) = 0.13; Thorlabs) directed the diffusely reflected laser light from the tissues to a single-photon counting module (Figure 1B).

To avoid crosstalk between the hs-NIRS and DCS signals, a shutter multiplexing system was used to rhythmically alternate between the respective light sources, achieving a sampling rate of 0.33 Hz for each modality. Measurements were taken from the scalp and hind limb for a total duration of 10 min, with PE or saline boluses administered after 2 min. Neon and reference light spectra (I_o) were acquired with both spectrometers for wavelength and intensity calibration, respectively. Dark measurements were taken for background noise subtraction from reference and tissue acquisitions.

2.3 | Data processing

2.3.1 | hs-NIRS analysis

The baseline reflectance (R) was calculated using custom scripts written in MATLAB, (Mathworks Inc., United States) for both spectrometers, taking into account their respective reference and dark signal spectra:

$$R(\lambda) = \log\left(\frac{I_{\text{tissue}}(\lambda) - I_{\text{dark}}(\lambda)}{I_0(\lambda) - I_{\text{dark}}(\lambda)}\right) \quad (1)$$

Subsequently, baseline chromophore concentrations and reduced scattering coefficients (μ_s'), Equations (2) and (3), were estimated by fitting the first and second spectral derivatives of $R(\lambda)$ to the corresponding derivatives of an analytical model, based on the solution to the diffusion equation for a semi-infinite homogeneous medium.[24,27–29]

$$\mu_a(\lambda) = \text{WF} \bullet \varepsilon_{\text{H}_2\text{O}} + \text{Hb} \bullet \varepsilon_{\text{Hb}} + \text{HbO} \bullet \varepsilon_{\text{HbO}} \quad (2)$$

$$\mu_s'(\lambda) = A\left(\frac{\lambda}{800}\right)^{-\alpha} \quad (3)$$

Subsequently, the differential pathlength factor (DPF) was calculated from baseline μ_a and μ_s' using Equation (4),[30] which was rescaled with a correction factor determined by fitting the second spectral derivative of $R(\lambda)$ to the second derivative of the water absorption spectrum.[26]

$$\text{DPF}(\lambda) = \frac{1}{2}\left(\frac{3\mu_s'(\lambda)}{\mu_a(\lambda)}\right)^{\frac{1}{2}}\left(1 - \frac{1}{1 + \rho\left(3\mu_a(\lambda)\mu_s'(\lambda)\right)^{\frac{1}{2}}}\right) \quad (4)$$

Using the wavelength-dependent DPF, changes in the chromophore concentrations (ΔHb and ΔHbO) were computed from the broadband attenuation spectra using

the modified Beer–Lambert Law. This approach provides reliable estimates of changes in tissue chromophore concentrations and is more computationally efficient than the derivative fitting. HbT was calculated as the sum of Hb and HbO. StO_2 was obtained from baseline (HbO, HbT) and time-dependent changes (ΔHbO, ΔHbT) in the chromophore concentrations:

$$StO_2(t) = 100\% \cdot \frac{HbO + \Delta HbO(t)}{HbT + \Delta HbT(t)} \tag{5}$$

2.3.2 | DCS analysis

Dynamic μ_a and baseline μ_s' at 785 nm from the hs-NIRS analysis were used to obtain blood flow indices (BFi) from DCS measurements (MATLAB, Mathworks Inc., United States) by fitting the experimental electric autocorrelation functions with an analytical model based on the solution to the correlation diffusion equation for a semi-infinite homogenous medium.[24,29,31,32] Relative blood flow (rBF) was computed as a percentage of the average BFi in the first 50 s (t_0):

$$rBF(t) = 100\% \cdot \frac{BFi(t)}{BFi(t_0)};$$
$$\Delta rBF(t) = 100\% \left(\frac{BFi(t)}{BFi(t_0)} - 1 \right) \tag{6}$$

Relative changes in vascular conductance[33] (ΔrC) was subsequently quantified for each microvascular bed (muscle or brain) using the rBF measurements:

$$\Delta rC(t) = \frac{C(t) - C(t_0)}{C(t_0)}$$

$$\Delta rC(t) = \frac{\frac{BF(t)}{MAP(t)} - \frac{BF(t_0)}{MAP(t_0)}}{\frac{BF(t_0)}{MAP(t_0)}}$$

$$\Delta rC(t) = \frac{BF(t)}{BF(t_0)} \cdot \frac{MAP(t_0)}{MAP(t)} - 1$$

$$\Delta rC(t) = rBF(t) \cdot \frac{MAP(t_0)}{MAP(t)} - 1 \tag{7}$$

where BF represents absolute blood flow.

2.3.3 | Statistical analysis

For consistency, each rat's responses to the first two injections of PE or saline were averaged. All data were assessed for normality through a visual inspection of a QQ plot and the Shapiro–Wilk test. Statistical analysis was conducted using GraphPad Prism version 9 (GraphPad Software Inc., San Diego), and statistical significance was defined as $p < 0.05$. For the period following the injection, the 3-s average around the point of maximum change in the time course was determined for the HbO, Hb, HbT, StO_2, rBF, and MAP. Additionally, the maximum increase and decrease in ΔrC were determined. For rBF, the area above and below 0 after injection were calculated as it was more representative of the positive and negative change present in the rBF time courses. To assess regulatory mechanisms responding to the effects of PE (i.e., secondary hemodynamic responses), the time constants from a kinetic exponential function[34,35] (i.e., time to reach 63% of maximum change) were fit to the rBF data. Further, the muscle and brain time constants were compared. An unpaired t-test was used to compare the responses to PE and saline injections for all parameters in both the muscle and brain.

3 | RESULTS

The hs-NIRS muscle measurements from all seven rats were successfully analyzed; however, three of the DCS datasets and corresponding hs-NIRS brain measurements were corrupted due to experimental errors. This reduced the sample size of the DCS and brain hs-NIRS to four rats, but with two injections per animal. Further, one of the saline injections for the DCS was excluded from the analysis due to motion artifacts.

Figure 2 shows the average muscle (Figure 2A,B) and brain (Figure 2C,D) chromophore (HbO, Hb, and HbT) responses to saline (Figure 2A,C) and PE (Figure 2B,D) injections. For the muscle (Figure 2A,B), the maximum changes in chromophore concentration were significantly different between saline and PE injections for HbO ($p \leq 0.0001$), Hb ($p \leq 0.01$), and HbT ($p \leq 0.0001$). Specifically, HbO changes were -0.25 ± 1.2 μM following saline injection and -3.1 ± 1.4 μM after PE administration. Hb changes were $\sim 0.01 \pm 0.31$ μM following saline injection and -0.33 ± 0.38 μM for PE injection. HbT changes were -0.13 ± 1.3 μM for saline injection and -3.3 ± 0.9 μM following PE injection. For the brain (Figure 2C,D), the maximum changes were significantly different for HbO ($p \leq 0.0001$) and HbT ($p \leq 0.008$), but not Hb ($p = 0.06$). Following saline and PE injections, respectively, HbO changes were -0.25 ± 1.2 μM and 4.2 ± 1.3 μM, Hb changes were 0.3 ± 0.8 μM and -1.0 ± 1.6 μM, and HbT changes were 0.1 ± 1.8 μM and 3.7 ± 2.8 μM.

Figure 3 shows the muscle (Figure 3A,B) and brain (Figure 3C,D) StO_2 responses to saline (Figure 3A,C) and
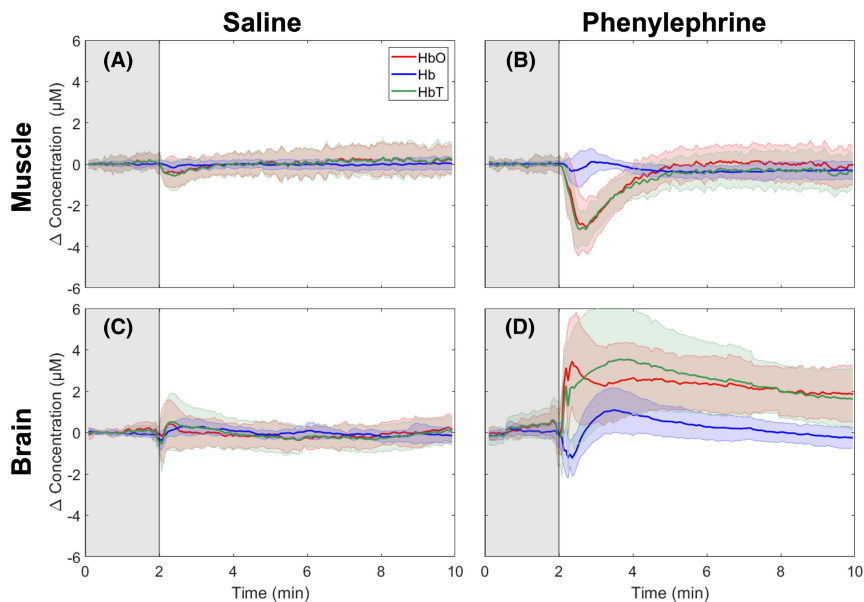
FIGURE 2 Δ HbO (red), Δ Hb (blue), and Δ HbT (green) responses to saline (A), (C) and PE (B), (D) administration after a 2-min baseline period (gray). Time courses are presented for (A), (B) muscle ($n = 14$ injections) and (C), (D) brain ($n = 8$). The time courses included two injections per rat. The shading surrounding each line represents the standard deviation.
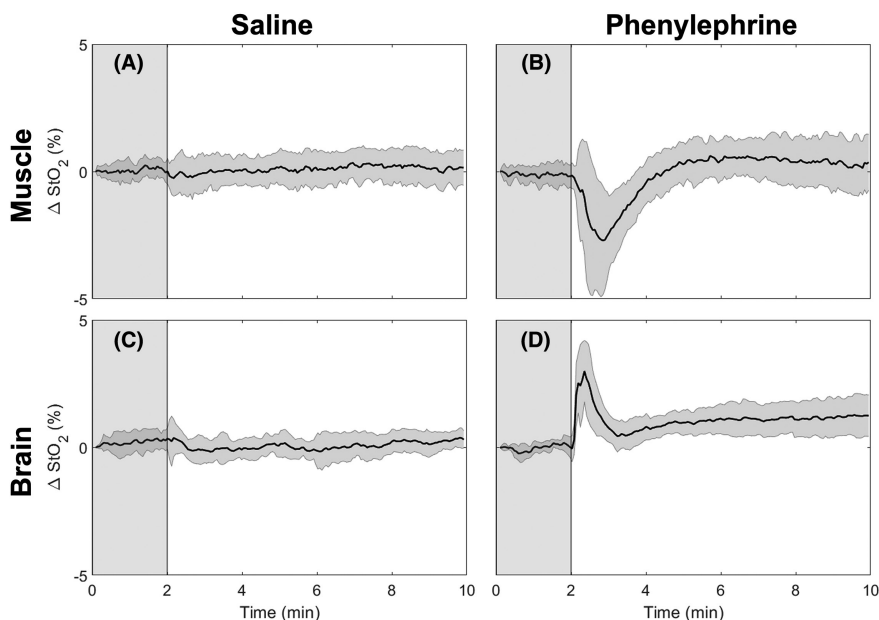

FIGURE 3 ΔStO_2 responses to (A), (C) saline and (B), (D) PE administration after a 2-minute baseline period (gray). Time courses are presented for (A), (B) muscle ($n = 14$) and (C), (D) brain ($n = 8$ injections). The time courses included two injections per rat. The shading surrounding each line represents the standard deviation.

PE (Figure 3B,D) injections. (Figure 3A,B), The maximum changes were significantly different in the muscle ($p \leq 0.009$) and brain ($p \leq 0.0001$) when comparing saline and PE injections. Specifically, average StO_2 changes were $0.02 \pm 1.3\%$ following saline injection and $-2.5 \pm 3.0\%$ for PE injection in the muscle. In the brain, the average StO_2 changes were $0.1 \pm 1.2\%$ for saline and $3.2 \pm 1.0\%$ following PE injection.

Figure 4 shows the MAP changes on the right y-axis following saline (Figure 4A,C) and PE (Figure 4B,D) injections. The average muscle (Figure 4A,B) and brain (Figure 4C,D) rBF responses to saline (Figure 4A,C) and PE (Figure 4B,D) injections are shown with the left y-axis. The maximum change in MAP was significantly different ($p \leq 0.001$) following saline (10 ± 5 mmHg) and PE (37 ± 9 mmHg) injections.

For the rBF in the muscle (Figure 4A,B), the maximum increase ($p \leq 0.01$) was significantly different between saline and PE injections, but the maximum decrease ($p = 0.1$) was not. Specifically, the maximum increase was $9 \pm 1\%$ following saline injection and $13 \pm 3\%$ after PE injection. The maximum decrease was approximately $-3 \pm 1\%$ for saline injection and $-8 \pm 8\%$ following PE injection. For the brain (Figure 4C,D), the maximum increase ($p = 0.6$) and decrease ($p = 0.07$) were not significantly different between saline and PE injections. The maximum increase was $14 \pm 2\%$ following saline injection and $17 \pm 11\%$ following PE injection. The

maximum decerase was approximately $-11 \pm 2\%$ following saline injection and $-16 \pm 5\%$ following PE injection.

Additionally, for the rBF in the muscle (Figure 4A,B), the average area above ($p = 0.1$) and below ($p = 0.4$) zero were not significantly different between saline and PE injections. Specifically, the average area above zero was 24 ± 14 a.u. following saline injection and 46 ± 29 a.u. after PE injection. The area below zero was approximately -5 ± 4 a.u. for saline injection and -8 ± 5 a.u. following PE injection. For the brain (Figure 4C,D), the average area above ($p \leq 0.02$) and below ($p \leq 0.002$) zero were significantly different following saline and PE injections. The average area above zero was 31 ± 13 a.u.

following saline injection and 15 ± 6 a.u. following PE injection. The area below zero was approximately -8 ± 4 a.u. following saline injection and -65 ± 30 a.u. following PE injection. Further, the kinetic model fitting revealed that the secondary cerebral response had a time constant of 0.30 min, while the muscular rBF exhibited a time constant of 0.92 min (see Appendix S1 for the model fitting results).

Figure 5 shows the ΔrC in response to saline (Figure 5A,C) and PE (Figure 5B,D) injections. The maximum decreases were significantly different ($p \leq 0.01$) when comparing saline and PE injections in both the muscle (Figure 5B) and brain (Figure 5D). Specifically, the
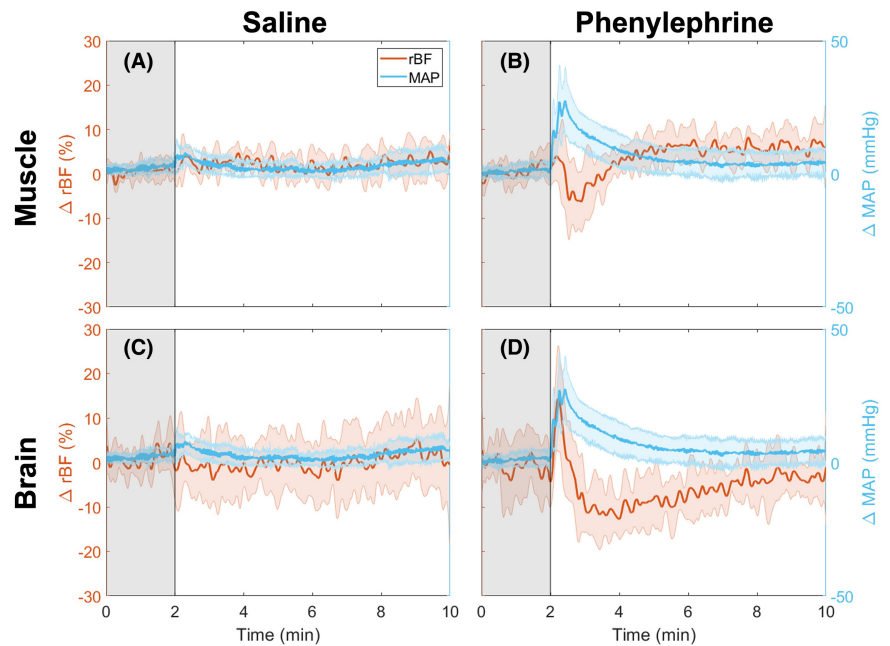

FIGURE 4 ΔrBF (orange) and ΔMAP (blue) responses to (A), (C) saline ($n = 5$ injections), and (B), (D) PE ($n = 6$) administration after a 2-min baseline period (gray). Time courses are presented for muscle (A), (B) and brain (C), (D). The time courses included two injections per rat, with the removal of one outlier injection. The shading surrounding each line represents the standard deviation.
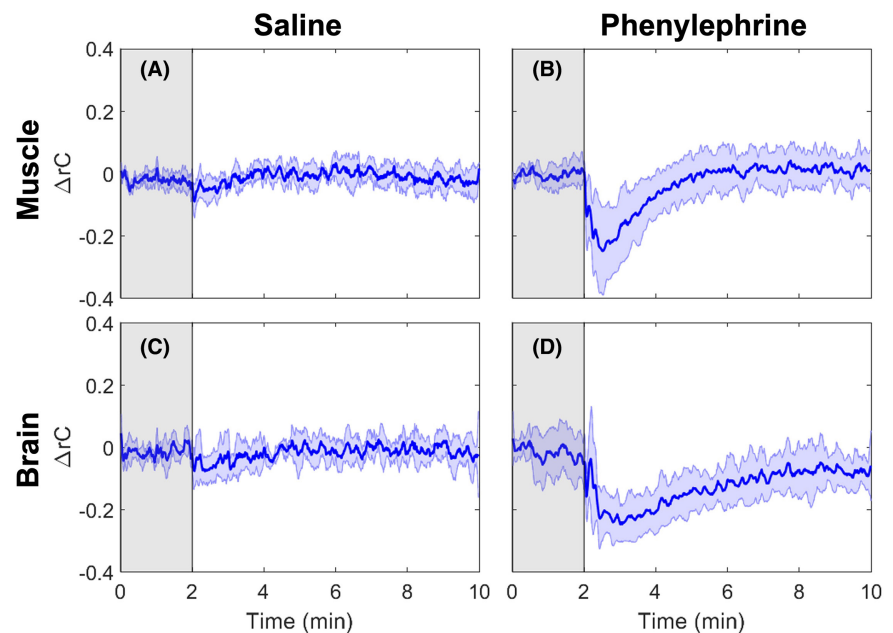

FIGURE 5 ΔrC responses to (A), (C) saline ($n = 5$ injections) and (B), (D) PE ($n = 6$) administration after a 2-min baseline period (gray). Time courses are presented for (A), (B) muscle and (C), (D) brain. The time courses included two injections per rat. The shading surrounding each line represents the standard deviation.

maximum decreases in the muscle were -0.12 ± 0.04 following saline injection and -0.3 ± 0.1 for PE. In the brain, the maximum changes were -0.16 ± 0.04 following saline injection and -0.29 ± 0.08 for PE. The maximum increases in response to saline or PE were not significantly different in either the muscle ($p = 0.1$) or the brain ($p = 0.09$).

4 | DISCUSSION

This study aimed to assess the effect of the same PE bolus on the skeletal muscle and brain microvascular beds. A hybrid hs-NIRS/DCS system was developed and used to concurrently monitor cerebral and skeletal muscle oxygenation and perfusion in Sprague–Dawley rats. In response to PE, the muscle showed an overall decrease in oxygenation and perfusion, while the brain showed an initial increase in both, followed by a decrease in perfusion from pre-injection baseline. These findings confirm our hypothesis that PE causes vasoconstriction in the skeletal muscle, but also reveal that the drug causes microvascular response in the brain.

Furthermore, PE administration led to significant increase in MAP compared to saline injection. PE is a common vasopressor; thus, this consistent and well-documented increase in MAP[36] further confirm the validity of our experimental protocol. In addition, the magnitude of the MAP increase following PE injection was similar to previously reported values in the same animal model.[37,38]

In the skeletal muscle, PE administration led to a significant decrease in HbO, HbT, and StO_2, as well as an increase in Hb and rBF. The skeletal muscle contains α-adrenergic receptors, which signal vasoconstriction following receptor binding of PE and, consequently, an initial decrease in blood volume, explaining the decrease in oxygenation and total hemoglobin. The observed peripheral response is consistent with skeletal muscle being the driving force of MAP increase following IV injection of PE, and these findings further agree with the understanding that increasing blood pressure through peripheral vasoconstriction shunts blood away from the muscle and towards the brain (where there is lack of α-adrenergic receptors).[39,40] While the muscle HbO, HbT, and StO_2 decreased immediately after PE administration, they all increased and returned to near-baseline levels within the measurement window. Furthermore, while muscular rBF exhibited a slight initial decrease and subsequent increase beyond the baseline, brain rBF exhibited the reverse trend, suggesting a brief period of blood flow redistribution after PE administration.

Interestingly, pairing rBF measurements with MAP revealed relative changes in vascular conductance, shedding light on the potential role of cerebral autoregulation. Notably, upon PE injection, rC and rBF decreased in the muscle due to the drug's vasoconstrictive effects on the peripheral microvasculature. With the shunting of blood from the muscle, cerebral rBF initially increased, although cerebral rC did not change. Following this initial increase in cerebral rBF, cerebral rC subsequently decreased, likely as an autoregulatory mechanism to manage the excess flow. Furthermore, fitting an exponential function to the secondary decrease in brain rBF and increase in muscular rBF revealed a quicker kinetic response in the brain to adjust flow.

It is noteworthy that a previous NIRS study reported an increase in skeletal muscle oxygenation in humans following PE administration.[41] However, the work used an INVOS 5100 commercial cerebral oximeter, which assumes a fixed arterial-to-venous ratio to make estimates of relative proportions of HbO and Hb.[42] Therefore, their observed increase in skeletal muscle oxygenation may be linked to a sudden increase in venous return. In the current work, spectral derivative was applied to hs-NIRS data spanning dozens of wavelengths, which allows for reliable estimation of the concentrations of oxygenated and deoxygenated hemoglobin in the skeletal muscle without the aforementioned assumption.

A benefit of the quasi-simultaneous monitoring of the two microvascular beds is that the response of each organ to the same bolus can be compared. In the brain, PE administration led to significant increase in HbO, HbT, and StO_2; however, Hb did not significant change, although this could be due to the study being underpowered for the latter physiological parameter ($p = 0.06$). The rBF response to PE injection was significantly different from saline response but exhibited a biphasic pattern, consisting of an increase followed by a decrease. The increased blood flow could be due to flushing of hemoglobin into the cerebral microvasculature as blood is pushed to the brain from the muscles and other organs by vasoconstriction of the peripheral microcirculation. However, these findings contrast with previous reports of cerebral desaturation following PE administration.[2,14] Nevertheless, a study using an invasive probe in humans[43] during craniotomy showed no change in cerebral oxygen saturation following PE administration. Further, work investigating frontal lobe oxygenation in humans with cerebral oximetry found a decrease in StO_2; simultaneously, ultrasonography revealed that the internal carotid artery flow (supplying the cerebral cortex) increased following PE administration while the external carotid artery flow (supplying superficial layers) decreased.[44] These differences in the brain and muscle responses were expected and could help explain the discrepancy in previously reported effects of PE administration on the cerebral microcirculation with cerebral

oximetry. Notably, extracerebral tissue contamination of commercial cerebral oximeters is a well-known problem and represents a challenge due to the potent vasoconstriction of PE on the superficial layers (i.e., scalp). Previous work examining the effect of phenylephrine on patients under anesthesia using time-resolved NIRS, a technique less sensitive to superficial contamination, showed only small decreases in cerebral oxygen saturation (<2%)[21] compared to larger values previously reported using continuous-wave NIRS (~10%). Importantly, our findings agree with recent work that also showed an increase in cerebral oxygenation in Sprague–Dawley rats.[40]

Although the brain is a vital organ that requires constant perfusion, cerebral hyperperfusion can lead to dangers such as cerebral hyperperfusion syndrome, hypertensive encephalopathy, and luxury perfusion syndrome, among others.[45] Consequently, autoregulatory mechanisms maintain cerebral blood flow constant despite changing cerebral perfusion pressures. If autoregulation is disrupted (either due to pathology or when autoregulatory limits are exceeded), large increases in cerebral blood volume can have negative consequences including elevated intracranial pressure, endothelial damage, blood–brain barrier disturbance, edema, and hemorrhage.

One limitation of this work was the use of pentobarbital, an anesthetic that has been linked to impaired cerebral autoregulation.[25,46] However, we found that cerebral hemodynamics increase with the sudden increase in MAP, but oxygenation and perfusion recover faster compared to MAP. This suggests that MAP was not driving the changes in cerebral hemodynamics and that cerebral autoregulation was intact. Additionally, in recent work showing similar findings,[40] isoflurane was used as the anesthetic. In general, use of anesthetics can also impair autoregulation in humans, as there is evidence suggesting that the effect of PE administration on awake humans leads to a larger decrease in cerebral saturation when compared with anesthetized subjects.[2] Cerebral autoregulation disturbances are important to assess and control, especially in clinical settings, because the brain does not store oxygen, and any disruption in blood flow could quickly result in tissue hypoxia.

Another limitation of this study was the smaller sample size for the brain versus the leg due to positioning errors leading to the device not probing the brain correctly in a few rats. This was discovered when the DCS data showed similar diffusion coefficients in the two microvascular beds, while the brain measurements should be distinctly higher than those of the muscle. This also resulted in a reduced sample size for the perfusion measurements.

Future work will investigate the microvascular response to PE in sick or otherwise unhealthy animals, as phenylephrine is most commonly used to restore normal blood pressure during hypotension. This might explain postoperative delirium linked with PE[47] or the lack of change in cerebral oxygenation using invasive oxygen probes in humans undergoing craniotomy.[43] Additionally, hemoglobin concentration did not return to baseline levels during the collection window, suggesting that the collection window should be extended to determine whether phenylephrine causes a lasting effect on hemoglobin and oxygen saturation levels. Furthermore, the potential difference in microvascular responses to infusion versus bolus PE injection would be an interesting question to investigate. Finally, translating this work to study the effect of PE in humans through methods less sensitive to extracerebral signal contamination such as time-resolved NIRS, MRI, and perfusion CT could be provide additional insights.

5 | CONCLUSION

A hybrid hs-NIRS/DCS system was developed and used to concurrently study the effects of the same PE bolus injection on the brain and skeletal muscle. The muscle showed decreased oxygenation and perfusion, whereas the brain showed the opposite, suggesting a redistribution of flow from the periphery to the cerebral circulation. Using hs-NIRS and DCS to simultaneously monitor cerebral and muscle hemodynamics during a PE injection provided new insights into its effects on different microvascular beds. This study further reveals the potential confounding effects of extracerebral signal contamination observed in previously reported cerebral desaturation events following PE injection.

AUTHOR CONTRIBUTIONS

L. Mawdsley was responsible for animal surgeries, as well as data collection and interpretation. R. Eskandari contributed to data analysis and interpretation, while preparing the manuscript draft with F. Kamar, who also contributed to statistical analysis and data interpretation. A. Rajaram and L. Yip adapted and built the optical monitoring system. N. Abayomi contributed to the data analysis code. S. Milkovich assisted with data collection by assisting with the animal surgery. K. St. Lawrence and J.L. Carson assisted with the study concept and data interpretation. M. Diop and C.G. Ellis directed the study concept, design, and data interpretation. All authors edited the manuscript draft and approved the final version.

CONFLICT OF INTEREST STATEMENT

DATA AVAILABILITY STATEMENT

ORCID

Rasa Eskandari https://orcid.org/0009-0001-6702-9110

REFERENCES

1. Rajanathan R, Pedersen TM, Thomsen MB, Botker HE, Matchkov VV. Phenylephrine-induced cardiovascular changes in the anesthetized mouse: an integrated assessment of in vivo hemodynamics under conditions of controlled heart rate. *Front Physiol*. 2022;13:831724. doi:10.3389/fphys.2022.831724

2. Meng L, Sun Y, Zhao X, et al. Effects of phenylephrine on systemic and cerebral circulations in humans: a systematic review with mechanistic explanations. *Anaesthesia*. 2023;10:71-85. doi:10.1111/anae.16172

3. Meng L, Cannesson M, Alexander BS, et al. Effect of phenylephrine and ephedrine bolus treatment on cerebral oxygenation in anaesthetized patients. *Br J Anaesth*. 2011;107(2):209-217. doi:10.1093/bja/aer150

4. Poterman M, Vos JJ, Vereecke HE, et al. Differential effects of phenylephrine and norepinephrine on peripheral tissue oxygenation during general anaesthesia. *Eur J Anaesthesiol*. 2015;32(8):571-580.

5. Maier S, Hasibeder WR, Hengl C, et al. Effects of phenylephrine on the sublingual microcirculation during cardiopulmonary bypass. *Br J Anaesth*. 2009;102(4):485-491. doi:10.1093/bja/aep018

6. Van Lieshout JJ, Secher NH. Last word on point:counterpoint: sympathetic activity does/does not influence cerebral blood flow. *J Appl Physiol*. 2008;105(4):1374. doi:10.1152/japplphysiol.91077.2008

7. Strandgaard S, Sigurdsson ST. Counterpoint: sympathetic nerve activity does not influence cerebral blood flow. *J Appl Physiol*. 2008;105(4):1366-1367. doi:10.1152/japplphysiol.90597.2008a

8. Hengstmann JH, Goronzy J. Pharmacokinetics of 3H-phenylephrine in man. *Eur J Clin Pharmacol*. 1982;21(4):335-341. doi:10.1007/BF00637623

9. Faraci FM, Heistad DD. Regulation of large cerebral arteries and cerebral microvascular pressure. *Circ Res*. 1990;66(1):8-17. doi:10.1161/01.RES.66.1.8

10. Heinonen I, Koga S, Kalliokoski KK, Musch TI, Poole DC. Heterogeneity of muscle blood flow and metabolism. *Exerc Sport Sci Rev*. 2015;43(3):117-124. doi:10.1249/JES.0000000000000044

11. Augustin HG, Koh GY. Organotypic vasculature: from descriptive heterogeneity to functional pathophysiology. *Science*. 2017;357(6353):eaal2379. doi:10.1126/science.aal2379

12. Kalmar AF, Allaert S, Pletinckx P, et al. Phenylephrine increases cardiac output by raising cardiac preload in patients with anesthesia induced hypotension. *J Clin Monit Comput*. 2018;32(6):969-976. doi:10.1007/s10877-018-0126-3

13. Fassaert LMM, de Borst GJ, Pennekamp CWA, et al. Effect of phenylephrine and ephedrine on cerebral (tissue) oxygen saturation during carotid endarterectomy (PEPPER): a randomized controlled trial. *Neurocrit Care*. 2019;31(3):514-525. doi:10.1007/s12028-019-00749-w

14. Brassard P, Seifert T, Wissenberg M, Jensen PM, Hansen CK, Secher NH. Phenylephrine decreases frontal lobe oxygenation at rest but not during moderately intense exercise. *J Appl Physiol*. 2010;108(6):1472-1478. doi:10.1152/japplphysiol.01206.2009

15. Meng L, Gelb AW, Alexander BS, et al. Impact of phenylephrine administration on cerebral tissue oxygen saturation and blood volume is modulated by carbon dioxide in anaesthetized patients. *Br J Anaesth*. 2012;108(5):815-822. doi:10.1093/bja/aes023

16. Foss VT, Christensen R, Rokamp KZ, Nissen P, Secher NH, Nielsen HB. Effect of phenylephrine vs. ephedrine on frontal lobe oxygenation during caesarean section with spinal anesthesia: an open label randomized controlled trial. *Front Physiol*. 2014;5:81. doi:10.3389/fphys.2014.00081

17. Milej D, Abdalmalak A, Rajaram A, St. Lawrence K. Direct assessment of extracerebral signal contamination on optical measurements of cerebral blood flow, oxygenation, and metabolism. *Neurophotonics*. 2020;7(4):045002. doi:10.1117/1.NPh.7.4.045002

18. Diop M, St. Lawrence K. Improving the depth sensitivity of time-resolved measurements by extracting the distribution of times-of-flight. *Biomed Opt Express*. 2013;4(3):447-459. doi:10.1364/boe.4.000447

19. Ogoh S, Sato K, Okazaki K, et al. A decrease in spatially resolved near-infrared spectroscopy-determined frontal lobe tissue oxygenation by phenylephrine reflects reduced skin blood flow. *Anesth Analg*. 2014;118(4):823-829. doi:10.1213/ANE.0000000000000145

20. Moerman AT, Vandenheuvel M, Tuybens PJ, Van Gompel C, De Hert SG. Incongruous effect of phenylephrine on changes in cerebral blood volume measured by near-infrared spectroscopy (NIRS) indicating extracranial contamination. *J Clin Monit Comput*. 2022;36(3):745-750. doi:10.1007/s10877-021-00702-3

21. Kamar F, Shoemaker LN, Eskandari R, et al. Assessing changes in regional cerebral hemodynamics in adults with a high-density full-head coverage time-resolved near-infrared spectroscopy device. *J Biomed Opt*. 2024;29(S3):S33302. doi:10.1117/1.JBO.29.S3.S33302

22. Mawdsley L. *Using Hyperspectral Near-Infrared Spectroscopy and Diffuse Correlation Spectroscopy to Monitor the Effects of Phenylephrine in the Microcirculation*. Master of Science. Western University; 2021.

23. Mawdsley L, Rajaram A, Yip L, et al. Simultaneous monitoring of the cerebral and skeletomuscular microcirculation using hyperspectral near infrared spectroscopy and Intravital video microscopy. *FASEB J*. 2021;35(S1). doi:10.1096/fasebj.2021.35.S1.00289

24. Rajaram A, Bale G, Kewin M, et al. Simultaneous monitoring of cerebral perfusion and cytochrome c oxidase by combining broadband near-infrared spectroscopy and diffuse correlation spectroscopy. *Biomed Opt Express*. 2018;9(6):2588-2603. doi:10.1364/boe.9.002588

25. Eskandari R, Milkovich S, Kamar F, et al. Assessing progressive microvascular dysfunction in early sepsis with non-invasive optical spectroscopy. *Optica Biophotonics Congress: Biomedical Optics 2024 (Translational, Microscopy, OCT, OTS, BRAIN)*. Optica Publishing Group; 2024. doi:10.1364/TRANSLATIONAL.2024.TW1B.3

26. Eskandari R. Assessing early microcirculatory changes in skeletal muscle and brain of a rat model of sepsis with hyperspectral

near-infrared and diffuse correlation spectroscopy. Electronic Thesis and Dissertation Repository. 2024 10114.

27. Kewin M, Rajaram A, Milej D, et al. Evaluation of hyperspectral NIRS for quantitative measurements of tissue oxygen saturation by comparison to time-resolved NIRS. *Biomed Opt Express*. 2019;10(9):4789-4802. doi:10.1364/boe.10.004789

28. Yeganeh HZ, Toronov V, Elliot JT, Diop M, Lawrence KS, Lee TY. Quantitative measurement of cerebral blood flow using broadband continuous wave near infrared spectroscopy. In: Digital Holography and Three-Dimensional Imaging, DH. 2012. doi:10.1364/biomed.2012.jm3a.3

29. Diop M, Kishimoto J, Toronov V, Lee DSC, St. Lawrence K. Development of a combined broadband near-infrared and diffusion correlation system for monitoring cerebral blood flow and oxidative metabolism in preterm infants. *Biomed Opt Express*. 2015;6(10):3907-3918. doi:10.1364/boe.6.003907

30. Scholkmann F, Wolf M. General equation for the differential pathlength factor of the frontal human head depending on wavelength and age. *J Biomed Opt*. 2013;18(10):105004. doi:10.1117/1.jbo.18.10.105004

31. Diop M, Verdecchia K, Lee TY, St Lawrence K. Calibration of diffuse correlation spectroscopy with a time-resolved near-infrared technique to yield absolute cerebral blood flow measurements. *Biomed Opt Express*. 2011;2(7):2068-2081. doi:10.1364/boe.2.002068

32. Rajaram A, Milej D, Suwalski M, et al. Optical monitoring of cerebral perfusion and metabolism in adults during cardiac surgery with cardiopulmonary bypass. *Biomed. Opt Express*. 2020;11(10):5967-5981. doi:10.1364/BOE.404101

33. Limberg JK, Casey DP, Trinity JD, et al. Assessment of resistance vessel function in human skeletal muscle: guidelines for experimental design, Doppler ultrasound, and pharmacology. *Am J Physiol Heart Circ Physiol*. 2020;318(2):H301-H325. doi:10.1152/ajpheart.00649.2019

34. Ward JL, Craig JC, Liu Y, et al. Effect of healthy aging and sex on middle cerebral artery blood velocity dynamics during moderate-intensity exercise. *Am J Physiol Heart Circ Physiol*. 2018;315(3):H492-H501. doi:10.1152/ajpheart.00129.2018

35. Billinger SA, Craig JC, Kwapiszeski SJ, et al. Dynamics of middle cerebral artery blood flow velocity during moderate-intensity exercise. *J Appl Physiol*. 2017;122(5):1125-1133. doi:10.1152/japplphysiol.00995.2016

36. Thiele RH, Nemergut EC, Lynch C. The clinical implications of isolated alpha1 adrenergic stimulation. *Anesth Analg*. 2011;113(2):297-304. doi:10.1213/ANE.0b013e3182120ca5

37. Talmor D, Roytblat L, Artru AA, et al. Phenylephrine-induced hypertension does not improve outcome after closed head trauma in rats. *Anesth Analg*. 1998;87(3):574-578. doi:10.1213/00000539-199809000-00014

38. Thurston CL, Helton ES. Effects of intravenous phenylephrine on blood pressure, nociception, and neural activity in the rostral ventral medulla in rats. *Brain Res*. 1996;717(1–2):81-90. doi:10.1016/0006-8993(96)00007-8

39. Harik SI, Sharma VK, Wetherbee JR, Warren RH, Banerjee SP. Adrenergic and cholinergic receptors of cerebral microvessels. *J Cereb Blood Flow Metab*. 1981;1(3):329-338. doi:10.1038/jcbfm.1981.36

40. CAS Annual Meeting Abstracts. *Can J Anesth*. 2023;70(S2):224-226. doi:10.1007/s12630-023-02651-8

41. Sørensen H, Thomsen JH, Meyer ASP, et al. Phenylephrine increases near-infrared spectroscopy determined muscle oxygenation in men. *J Clin Monit Comput*. 2017;31(6):1159-1166. doi:10.1007/s10877-016-9965-y

42. Grocott HP. Phenylephrine and paradoxically increased muscle tissue oxygenation: is the mechanism related to local venoconstriction or augmented venous return? *J Clin Monit Comput*. 2018;32(6):1143. doi:10.1007/s10877-018-0102-y

43. Pedersen SS, Meyhoff CS, Olsen MH, et al. Impact of hyperoxia and phenylephrine on cerebral oxygenation: an experimental clinical study. *Acta Anaesthesiol Scand*. 2023;67(1):57-65. doi:10.1111/aas.14149

44. Sørensen H, Rasmussen P, Sato K, et al. External carotid artery flow maintains near infrared spectroscopy-determined frontal lobe oxygenation during ephedrine administration. *Br J Anaesth*. 2014;113(3):452-458. doi:10.1093/bja/aet481

45. Delgado MG, Bogousslavsky J. Cerebral Hyperperfusion syndrome and related conditions. *Eur Neurol*. 2020;83(5):453-457. doi:10.1159/000511307

46. Wang Z, Schuler B, Vogel O, Arras M, Vogel J. What is the optimal anesthetic protocol for measurements of cerebral autoregulation in spontaneously breathing mice? *Exp Brain Res*. 2010;207:249-258. doi:10.1007/s00221-010-2447-4

47. Ma H, Ahrens E, Wachtendorf LJ, et al. Intraoperative use of phenylephrine versus ephedrine and postoperative delirium: a multicenter retrospective cohort study. *Anesthesiology*. 2023;140:657-667. doi:10.1097/aln.0000000000004774

SUPPORTING INFORMATION

Additional supporting information can be found online in the Supporting Information section at the end of this article.